How sediment promotes narrow rifting: Application to the Gulf of California

Robert W. Bialas[1] and W. Roger Buck[1]

Received 18 September 2008; revised 9 March 2009; accepted 13 May 2009; published 22 August 2009.

[1] If the gravitational stress changes related to crustal thinning are large enough to affect the mode of extension, then sedimentation should also affect that mode. We propose that the weight of sediments reduces the difference in crustal buoyancy forces caused by local crustal thinning, allowing a rift to extend more easily in a narrow rift mode. We examine the effect of deposition of large amounts of nonlocally derived sediment on extensional style using two-dimensional, regional-scale numerical experiments of extending thick continental crust with varied initial thermal conditions, geometries, rheological parameters, and sedimentation properties. Depending on initial model conditions, the onset of rifting in thick continental crust occurs in the narrow rifting, wide rifting, or core complex mode. With continued extension, all cases eventually transition to a narrow rifting mode. For a system in wide rift mode, moderate to fast sedimentation shortens the time needed to transition to a narrow rift. In the Gulf of California, changes in extensional style correlate with sediment thickness, with an earlier transition to narrow rifting in the north versus the south. We compare our model results to the extensional history of the Gulf of California, where sediments may have caused the northern and north central domain of the gulf (Delfin-Tiburon and Guaymas segments) to transition to narrow rifting before the south central domains (Alarcon segment). **Citation:** Bialas, R. W., and W. R. Buck (2009), How sediment promotes narrow rifting: Application to the Gulf of California, *Tectonics*, *28*, TC4014, doi:10.1029/2008TC002394.

1. Introduction

[2] Sediments are one of the main recorders of tectonic events, but they may also affect the way compression or extension proceeds. It is now accepted that the unloading effect of erosion can change the pattern of compressional deformation in areas of continental convergence [e.g., *Willett et al.*, 1993; *Beaumont et al.*, 2004]. In a similar way, we suggest that the load of sediments may promote localized deformation in areas of continental extension. Recently collected data from the Gulf of California [*Lizarralde et al.*, 2007] indicates that higher rates of sedimentation are associated with a switch from distributed, or wide rift style, extension to more focused, narrow rift style, extension.

[3] Study of the role of sediments in continental extension may help resolve the question of what controls whether extension is localized or distributed. Extensional stretching should thin the lithosphere [e.g., *McKenzie*, 1978] and the strength of the lithosphere depends on its thickness [e.g., *Brace and Kohlstedt*, 1980]. Thus, extensional deformation might be expected to focus in the area of thinnest, weakest lithosphere. However, a number of regions, including the Basin and Range Province of western North America and the Aegean, have extended over a very wide region [e.g., *Noble*, 1941; *Hamilton*, 1987; *Makris*, 1978].

[4] Two models have been suggested to explain the difference between wide and narrow rifts. The first considers the strength of the lithosphere and how it is affected by the rate of extension. If the creep strength of continental crust is less than mantle lithosphere, as suggested by laboratory measurements [e.g., *Kirby and Kronenberg*, 1987], then very slow extension could lead to strengthening of the lithosphere and then to wide rifting [*England*, 1983; *Sonder and England*, 1989]. The second model considers the relative change of buoyancy-related forces compared to lithospheric strength [*Buck*, 1991]. The thinning of low-density crust produces gravitational stresses, which can be summed to give a buoyancy force change, that make continued extension harder. If the increase in buoyancy force difference is greater than the lithospheric strength reduction, then a wide rift should result.

[5] The addition of sediments to an evolving rift should affect both the crustal buoyancy force and the lithospheric thermal and strength structure. Sediments should reduce the magnitude of the crustal buoyancy force change during extension, since crustal thinning is offset by addition of sediments. The effect of sediments on the evolving thermal structure is less clear. *Lizarralde et al.* [2007] propose that sediments should warm the lithosphere due to a ''thermal blanketing'' effect. However, the addition of cold sediments could push isotherms down and lead to strengthening of a rift.

[6] In this paper, we describe numerical model calculations that investigate how sedimentation affects the mode of extension. The effects of erosion of rift flanks and sedimentation in rift basins have previously been studied using numerical models of lithosphere extension [*Avouac and Burov*, 1996; *Burov and Poliakov*, 2001]. Two things make

[1]Lamont-Doherty Earth Observatory, Earth Institute at Columbia University, Palisades, New York, USA.

0278-7407/09/2008TC002394

our models different from these studies: (1) we consider nonlocally sourced sediments, delivered from the far field by rivers; and (2) we are interested in the transition between wide and narrow mode extension. By varying the rate of addition and the density of sediments added to numerical model rifts we should be able to clarify the role sediments may play in controlling the style of rifting. Specifically, we document how sedimentation changes the time of onset of narrow rifting for cases with different initial conditions. We explore a wide range of model parameters, altering not only the initial thermal and crustal structures, but also many of the variables involved in sedimentation including the sediment density, sedimentation rate, and style of sedimentation. We conclude by comparing our numerical results to geological and geophysical data from the Gulf of California, which motivated this study.

1.1. Wide Rifting

[7] Wide rifts occur in regions where orogeny has produced thicker than normal crust. The ~800 km wide Basin and Range Province has extended by about a factor of 2 since convergence ceased about 60 Ma B.P. [*Wernicke*, 1981]. Given that the present crustal thickness is ~30 km, the preextension crustal thickness must have been ~60 km thick. Thus it is likely that the region was a high plateau, similar in elevation to the Peruvian Altiplano or Tibet, before extension thinned the crust. The present heat flow in the Basin and Range Province is more than twice the average for continental crust [*Lachenbruch and Sass*, 1977]. Likewise the distributed extension of Aegean and the West Antarctic Rift System occurred in areas where convergence predated extension [e.g., *Dewey and Segnor*, 1979; *Goodge*, 2002, and references therein].

[8] A number of numerical model studies that do not treat sediments suggest that the initial crustal thickness and thermal structure of lithosphere influence the mode of rifting [e.g., *Buck*, 1991; *Bassi et al.*, 1993]. Distributed rifting seems to require hot, thin lithosphere and thicker-than-normal crust, while initially narrow rifts require cold, thick lithosphere [*Buck*, 1991; *Buck et al.*, 1999]. Model cases that start in the wide rift mode can naturally transition into the narrow rift mode [*Hopper and Buck*, 1996; *Bialas et al.*, 2007]. The cause of the transition in these models is complex. One view is that the transition occurs when the crust is thinned everywhere enough that crustal buoyancy changes (that scale with crustal thickness) become so small so that lithospheric thermal weakening dominates [e.g., *Hopper and Buck*, 1996].

[9] An alternative view is that evolving thermal effects may cause migration of the locus of rifting. Although this idea was first investigated with models that did not treat the gravitational stresses produced by crustal thinning [e.g., *England*, 1983; *Sonder and England*, 1989], more complete numerical models seem to indicate a central role of lithospheric cooling and strengthening in promoting wide rifting [e.g., *Lavier and Buck*, 2002; *Huerta and Harry*, 2007]. The transition from wide to narrow rifting may be controlled by thermal weakening of the crust at the rift edges [*Huerta and Harry*, 2007].

1.2. Conceptual Model

[10] Sediment may have an effect on the evolution of crustal buoyancy and lithospheric thermal structure during continental extension. If wide rifting is related to dominance of the crustal buoyancy force change, then addition of sediment should promote focused narrow rifting in lieu of wide rifting. The weight of the sediments reduces the crustal buoyancy force change, caused by local crustal thinning, allowing the thermal weakening to force the system into a narrow rift mode. Figure 1 provides a rough sketch of this concept. As a region of hot, thick crust extends without sediment, the buoyancy force difference from the rift edge to the center of the rift is large (represented in Figure 1 by arrow size). Rifting migrates out with the plateau edge. When large amounts of sediment are added, the crust is thickened from the top as it is thinned by strain. The force difference between the rift edge and the middle of the rift remains small and rifting does not migrate.

[11] Figure 2 outlines a geological scenario that could produce changes in the style of extension along strike of an extending region. With the onset of rifting in an area of thick continental crust, a core complex or wide rifting mode initiates. Extension lowers the surface elevation, and rivers transport sediment to the basins. However, sediment is not deposited evenly throughout the system, with deltaic areas receiving larger sediment influxes. Large volumes of sediment reduce the crustal buoyancy difference, changing the extensional style. Sediment rich areas are forced toward narrow rifting (Figure 1, right), while sediment poor regions continue in wide rift mode (Figure 1, left). With further extension, the whole basin shifts to narrow rift (Figure 2).

[12] We propose that a large influx of sediment may force a wide rift to transition into a narrow one. The numerical model we applied to this problem will allow us to investigate the range of conditions where this concept is plausible.

2. Model Description

[13] We examine the effect of deposition of nonlocally derived sediment on extensional style using highly idealized, regional-scale, two-dimensional numerical models. In all models, we consider extension of an isostatically compensated plateau. Modeling plateau extension has previously been applied to wide rifts such as the Basin and Range Province [*Harry et al.*, 1993] and the West Antarctic Rift System [*Huerta and Harry*, 2007; *Bialas et al.*, 2007]. A plateau scenario provides the hot, thick crust possibly required for core complex and wide rifting. Keeping the plateau area in the middle of the model domain prevents rifting from localizing at the edge of the model domain. For the standard case the isostatically compensated plateau is 3 km high with 52 km thick crust. A small plateau, 136 km wide, is used in most cases, as its associated model domain is small enough to allow runs to be completed in a reasonable amount of time, and it adequately displays transitions between different extensional styles. Off the plateau, crustal thickness grades at the sides over 20 km to normal crust of 32 km thick in all cases. Deformation is tracked using an explicit finite element method similar to

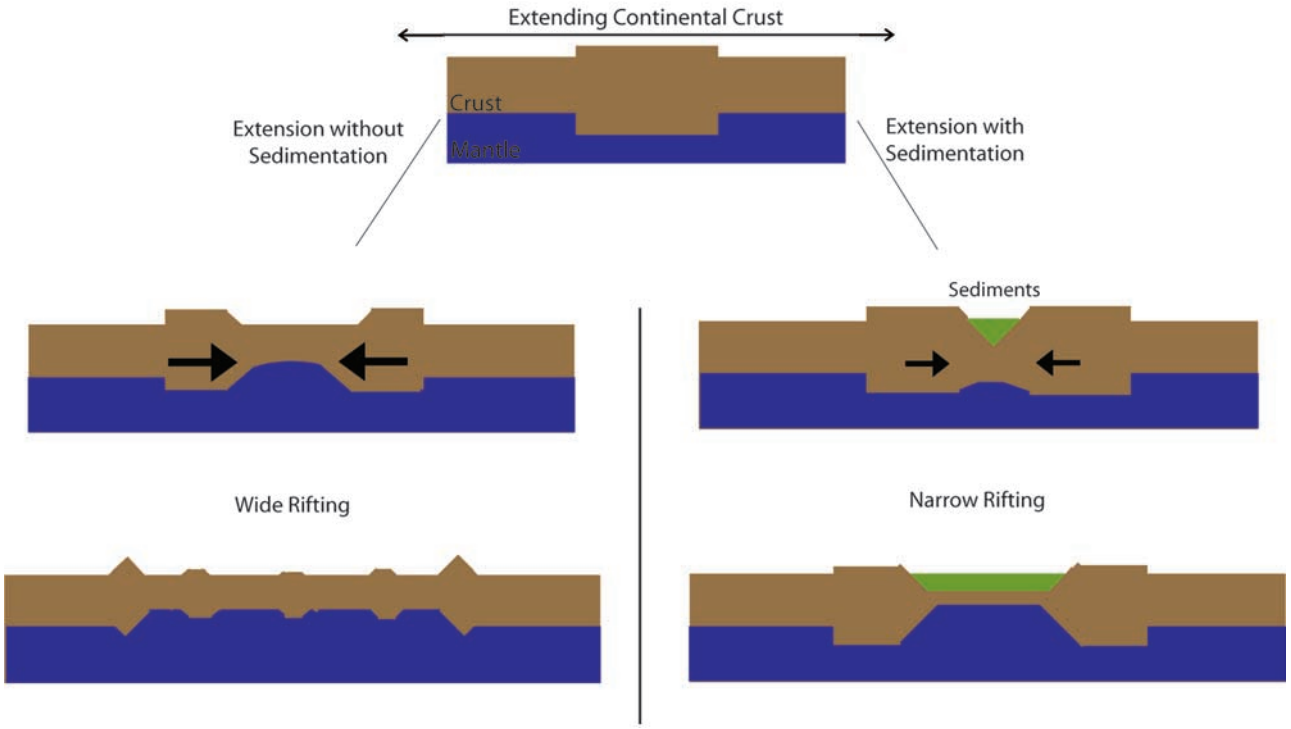

Figure 1. Cartoon illustrating our concept. Arrows in the middle level represent the size of the buoyancy force difference. Without sedimentation, buoyancy force differences are large, and the system extends as a wide rift. With sedimentation, the crust is thickened from the top as it is thinned, reducing the difference in crustal buoyancy force and extending as a narrow rift.

the fast Lagrangian analysis of continua (FLAC) technique [*Lavier et al.*, 2000, and references therein]. (A description of the numerical model is given in Appendix A.)

2.1. Sedimentation Description

[14] Our model deposits sediment from a third, lateral dimension, making this what is sometimes referred to as a 2.5-dimensional model [e.g., *Lavier and Bennett*, 2006] but uses a similar method of depositing it as other codes have for erosion [*Avouac and Burov*, 1996]. We ignore erosion as we wish to focus on the effects of sedimentation from the far field. Erosion changes the system by adding erosional denudation, reducing thicker areas of crust nontectonically and affecting isotherms.

[15] Once a surface element has dropped below a critical depth, sediment is added by increasing the surface height. The rheology of the sediment is the same as the crust but with a lower density. As the volume of sediment is initially small compared to the volume of rock for a particular element, the amount of sediment is tracked explicitly and the element's rheology is initially represented by a weighted average of the sediment and rock phases, until such time as sediment may occupy the entire volume of the element. The code isostatically adjusts the stresses and subsequent topography in the time steps following the addition of sediment.

[16] Two different ways of distributing the sediment were tested. For the majority of tests, a "uniform" delivery was used, in which sediment is added at a set rate once the surface drops below a set critical elevation. The sedimentation is stopped if the surface is shallower than the critical depth. In the second, "focused" approach, sediment is only deposited in the lowest point and the adjacent 4 grid elements.

2.2. Varied Model Parameters

[17] Table 1 outlines how 8 parameters were varied among 123 different experiments. Though our goal is to investigate the influence of sediment, we altered additional parameters to elucidate the conditions where sedimentation may have an effect. Results from models with changes in plateau dimensions and model resolution agreed with those from our "standard" case. Herein we present examples demonstrative of the model behavior over the entire range of model parameters. Each experiment is considered to have two parts: (1) the model with sedimentation and (2) a base model with the same nonsedimentation parameters (e.g., initial concentration of radiogenic elements, extension rate, plateau thickness, plateau width, and resolution) and sedimentation turned off.

3. Results

[18] Three extensional modes, narrow rifting, wide rifting, and core complex mode, were observed across the suite

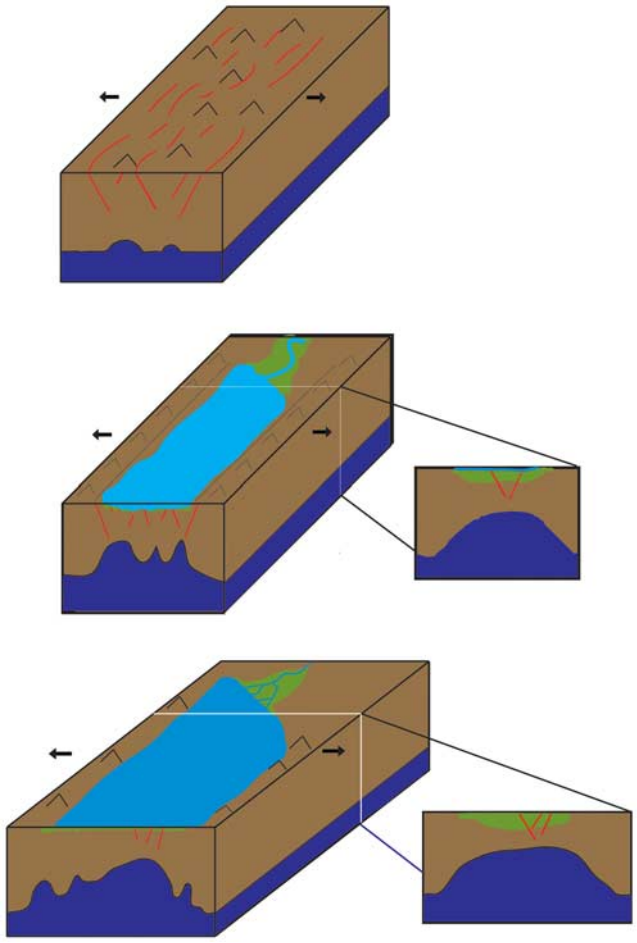

Figure 2. Cartoon illustrating conceptual geological model development. (top) The system begins rifting in core complex and wide rifting mode. (middle right) As extension continues, large amounts of sediment are deposited in part of the basin, forcing it into a narrow rift. (middle left) In the sediment starved areas, wide rifting continues. (bottom) Eventually, the entire rift transitions to a narrow rift. Color scheme: light blue, water; green, sediments; brown, crust; dark blue, mantle; red, active faults.

of models. Figure 3 presents type examples of these three modes. Core complex mode is defined as a period of focused extension in the upper crust with diffuse extension in the lower crust and upper mantle. Hot, low-viscosity lower crust is needed for core complex mode. Wide rifting is defined as a period with multiple zones of extension in the upper and lower crust. A model is considered to be in a narrow rift mode when strain is localized in one area through the entire section of lithosphere with strain rates an order of magnitude higher than in the rest of the model domain.

3.1. Example Model

[19] We present time slices from a model simulation (Figure 4) that is demonstrative of the majority of model cases and clearly shows the main changes in extensional style observed with the addition of sedimentation. Figure 4 shows the base model without sedimentation on the left and the model with sedimentation added on the right. Besides parameters controlling sedimentation, no other parameters are varied between the base model on the left and the sedimentation model on the right. Time slices of crustal structure, strain rate, and temperature are shown for both the base and sedimented models in each case.

[20] In the example (Figure 4), the initial Moho temperature, T_m, is 748°C. At the top left, the initial crustal and thermal cross sections are shown with a parameter list on the right. Time slices are the same for each half and were chosen to illustrate the key changes in extensional mode for both the base and sedimented model. In Figure 4b (left), the model without sedimentation undergoes core complex rifting, shown at 2.5 Ma. Core complex mode is followed by a long period of wide rifting with strain focused at the plateau edges, shown at 5 Ma. At 10.75 Ma, narrow rifting initiates when the low-viscosity root has been completely thinned out.

[21] Figure 4b (right) shows the model under the same conditions with sediment delivered uniformly at 3 m ka^{-1}. Extension begins in core complex mode through 4 Ma, similar to the model without sedimentation. Wide rifting begins at ~4 Ma but is short lived. Narrow rifting has begun to develop in the 5 Ma time slice, and the model is fully narrow at 5.25 Ma. Ample hot, low-viscosity lower crust remains under the plateau edge, but extension is no longer focused there. The 10.75 Ma time slice is shown to compare with the base model. Narrow rifting has persisted in this same location since 5 Ma. In this example, sedimentation at a high rate has driven the system to transition to a narrow rift 5.75 Ma earlier than its sediment starved counterpart.

[22] Model cases with sufficient sedimentation (in most cases at least 1 m ka^{-1}) and with moderate initial thermal structures (650°C < T_M < 1100°C) behave in a similar way to example 1. With a very hot initial thermal structure (T_M > 1100°C), the model remains in core complex mode; with a very cold initial thermal structure(T_M < 650°C), rifting initiates and persists as a narrow rift for the duration of the model [*Bialas et al.*, 2007]. Sedimentation has little to no affect on extensional style in these cases. However, when the base model (without sedimentation) transitions from core complex to wide rifting to narrow rifting, sedimentation influences the extensional mode.

3.2. Summary Diagrams

[23] All models eventually transition to narrow rifting. To illustrate how the time to narrow rifting changes, the time to narrow rifting for a model with sedimentation is subtracted from that of its comparative base model. This difference, time difference to narrow rifting (TDNR), is used Figures 5 and 6 depicting results from the entire suite of models.

[24] The onset of narrow rifting was determined by visual inspection of the normalized strain rate plots as the time slice when strain is localized through the entire section of lithosphere in one area by an order of magnitude greater than the rest of the model domain. When the model

Table 1. Model Parameters

Model Type	Number[a]	Parameters Changed	Parameters Held Constant
Standard	66	Sedimentation rate (0.1–5 m ka^{-1}) H_0, surface concentration of radiogenic elements (0–1.7 × 10^{-9} W kg^{-1})	Extension rate 2 cm a^{-1} Plateau thickness 52 km Plateau length 136 km Resolution 4 km grid Sedimentation density 2400 kg m^{-3} Sedimentation type uniform
Density test	26	Sediment density (500–2800 kg m^{-3})	Extension rate 2 cm a^{-1} Sedimentation rate 3 m ka^{-1} Plateau thickness 52 km Plateau width 136 km Resolution 4 km H_0, surface concentration of radiogenic elements 9 × 10^{-10} W kg^{-1} Sedimentation type uniform
Resolution test	7	Resolution 2 km grid Sedimentation rate (1–3 m ka^{-1}) H_0, surface concentration of radiogenic elements (0.5–1.5 × 10^{-9} W kg^{-1})	Extension rate 2 cm a^{-1} Plateau thickness 52 km Plateau width 136 km Sediment density 2400 kg m^{-3} Sedimentation type uniform
Plateau thickness test	8	Plateau thickness: (44–48 km) H_0, surface concentration of radiogenic elements (0–1.5 × 10^{-9} W kg^{-1})	Sedimentation rate 2 m ka^{-1} Extension rate 2 cm a^{-1} Plateau width 136 km Resolution 4 km grid Sediment density 2400 kg m^{-3} Sedimentation type uniform
Plateau width test	5	Plateau width 300 km H_0, surface concentration of radiogenic elements: (0.3–1 × 10^{-9} W kg^{-1})	Sedimentation rate 2 m ka^{-1} Plateau thickness 52 km Resolution 4 km grid Sediment density 2400 kg m^{-3} Sedimentation type uniform
Sedimentation style test	11	Sedimentation rate (0.1–5 m ka^{-1}) H_0, surface concentration of radiogenic elements (0–1.7 × 10^{-9} W kg^{-1}) Sedimentation style focused	Extension rate 2 cm a^{-1} Extension rate 2 cm a^{-1} Plateau thickness 52 km Plateau width 136 km Resolution 4 km grid Sediment density 2400 kg m^{-3}

[a]Total number 123.

remeshes, it takes a few time steps to return to a state of equilibrium. Model outputs close to the time of remeshing can appear erratic, and the model only outputs every 0.25 Ma. An error of ±0.25–0.5 Ma is therefore assumed from the visual inspection. One drawback for this method is it does not detect the start of narrow rifting. The narrow rift is only defined here after it is clearly the dominant form of extension.

[25] Sediment density also systematically affects model results. Figures 5a and 5b show raw time to narrow rifting TNR and derived TDNR plotted against sediment density for a model with T_m = 748°C and a uniform sedimentation rate of 3 m ka^{-1}. At low sediment densities, the extended regions are not sufficiently depressed to create enough accommodation space to continue sedimentation at the preset rate. The sediment piles up to the critical elevation for activating sedimentation, after which time, the sedimentation stops. A small volume of low-density sediment leads to little to no change in TDNR. As sediment density increases, the sediments depress the crust more, and TDNR increases linearly with sediment density. At higher densities, the TDNR levels off as the TNR bottoms out at about 5 Ma, similar to the TNR of models with varying T_M and high (3 m ka^{-1}) sedimentation rates (Figure 6a). At these high densities, the sedimented models have reached their largest possible value of TDNR as they must still pass through core complex stage before transitioning to wide and then quickly to narrow rifting. With increasing sediment load, TDNR increases until achieving its maximum.

[26] TNR and TDNR are shown in Figures 6a and 6b, respectively, for experiments with sedimentation rates of 0.5, 1, and 3 m ka^{-1} and varied initial thermal properties. The location of the example models shown in Figures 4 and 5 are indicated with arrows. At low values of Moho temperature, T_m, all models exhibit narrow rifting characteristics early in the calculation, leading to no difference in TDNR.

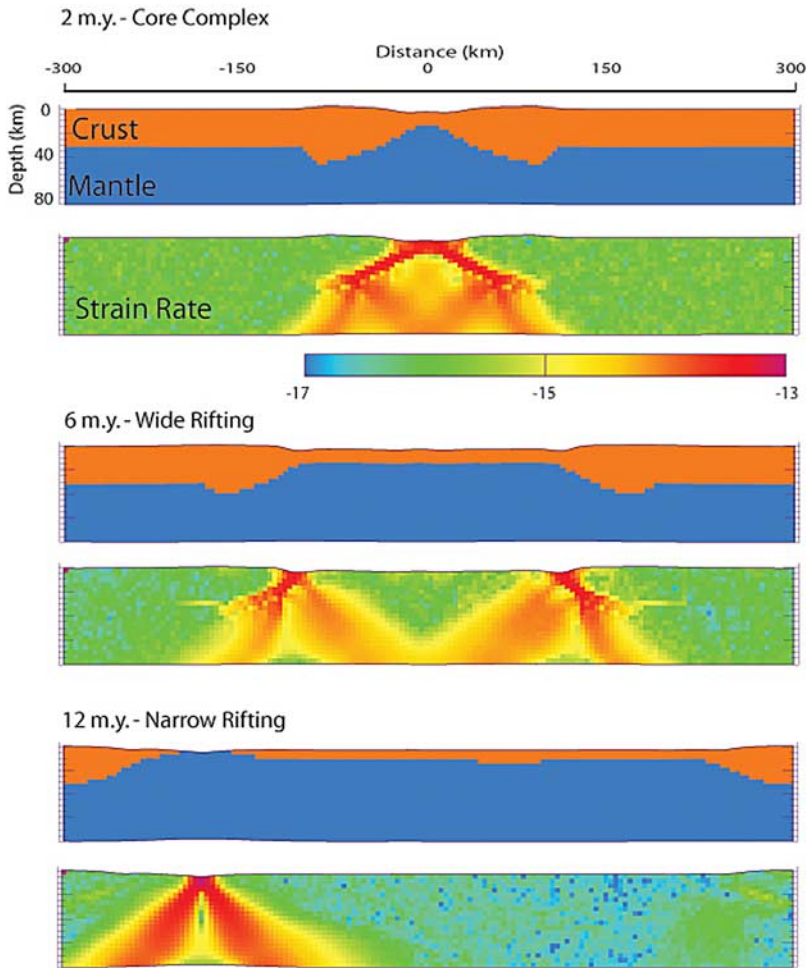

Figure 3. Plots of crustal structure and strain rate are presented for type examples of the three extensional modes observed here. At 2 Ma, core complex mode is observed. Wide rifting is shown in the 6 Ma time slice. Extension is focused at the plateau edges with minor extension in yellow observed in the upper crust (top 2–3 pixels) in the central extended region. The 12 Ma time slice shows an example of narrow rifting. Extension is symmetric and localized in one area through the entire depth of the model. Notice the blue mantle has begun to spread at the surface, indicating a crustal accretion phase.

With increasing temperature, TNR for the base model increases with increasing Moho temperature between about 650°C and 800°C, with the models spending longer in the wide rifting phase (Figure 6a, filled black circles). With rising temperatures from 650°C to 800°C, more of the lower crust of the plateau is weak. At 800°C, the entire lower crust of the plateau is weak, hence at higher temperatures, the supply of lower crustal material has not increased, and the TNR remains around 11–12 Ma.

[27] Sedimentation rate has a great effect on model results. At a sedimentation rate of 3 m ka^{-1}, models that would pass through a wide rift phase quickly transition to narrow rifting around 5 Ma. Slower sedimentation rates track closer to the base model. At 1 m ka^{-1}, a large difference is not observed until $T_M > 750$°C. At 0.5 m ka^{-1} and similar low sedimentation rates, sedimented models are similar to their base models until high T_M, again starting at above 750°C. At low sedimentation rates and the higher T_M, however, the sedimented models take longer, shown in Figure 6b as a negative TDNR.

[28] Example 2 (Figure 7) shows different simulation where the addition of sediment does not drive the system to a narrow rift earlier, but rather keeps the system in wide rifting mode. T_M is 805°C, and sediment is delivered uniformly at 0.5 m ka^{-1}. In the base model at left, extension progresses similar to the base model in Figure 4. At 2.5 Ma, core complex is observed, which transitions to wide rifting around 4 Ma. Wide rifting continues through until about 12 Ma. In the 12 Ma time slice shown, the model has almost completed the transition to narrow rifting.

[29] In contrast, the sedimented model in Figure 7, with a slightly hotter initial thermal structure and lower sedimentation rate, tells a very different story from that of Figure 4. The model begins in core complex mode and transitions to a wide rift around 4 Ma similar to that of Figure 4 and the base model. However, here the sedimented models of

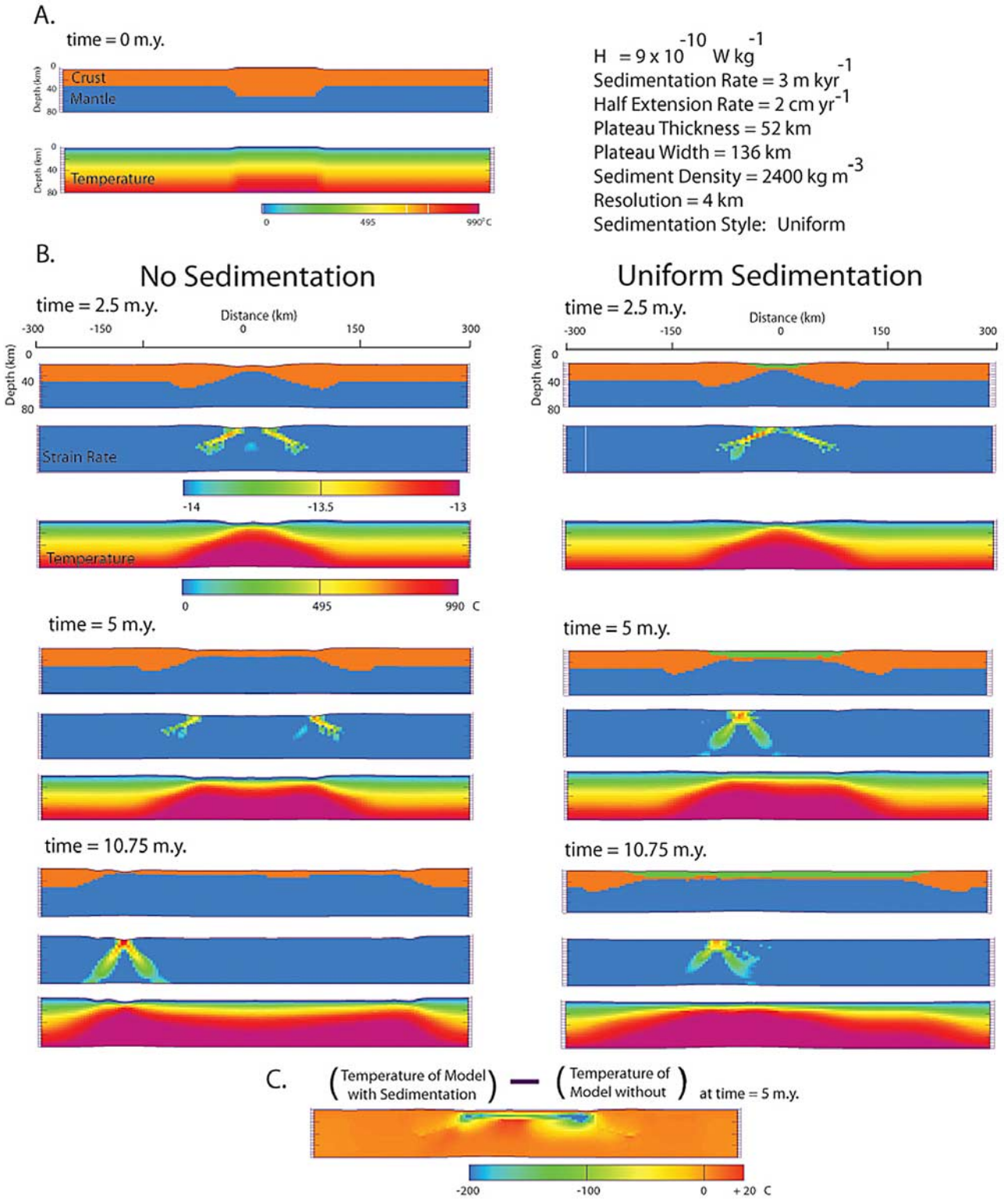
A.
time = 0 m.y.
Crust
Mantle
Temperature
0
495
990°C
H = 9 x 10^-10 W kg^-1
Sedimentation Rate = 3 m kyr^-1
Half Extension Rate = 2 cm yr^-1
Plateau Thickness = 52 km
Plateau Width = 136 km
Sediment Density = 2400 kg m^-3
Resolution = 4 km
Sedimentation Style: Uniform
B.
No Sedimentation
Uniform Sedimentation
time = 2.5 m.y.
Distance (km)
-300
-150
0
150
300
Depth (km)
Strain Rate
-14
-13.5
-13
Temperature
0
495
990 C
time = 5 m.y.
time = 10.75 m.y.
C.
(Temperature of Model with Sedimentation) — (Temperature of Model without) at time = 5 m.y.
-200
-100
0
+20 C

Figure 4

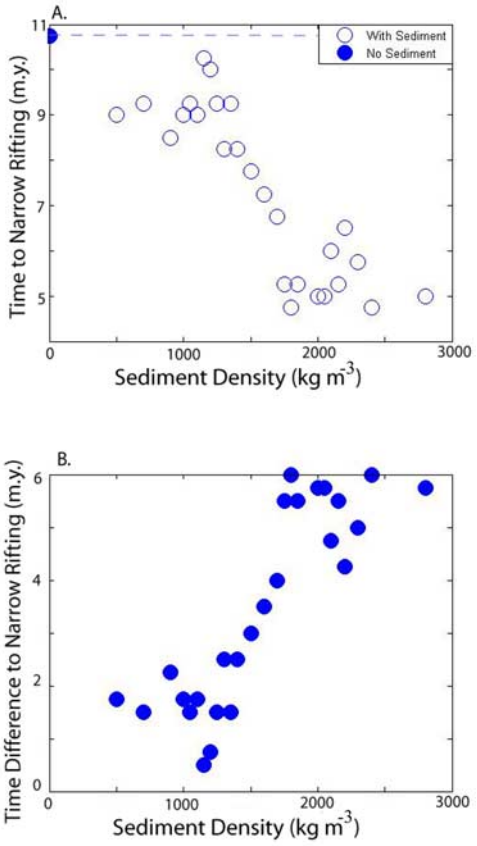

Figure 5. (a) Plot of time to narrow rifting (TNR) for series with varied sediment density (open circles). The base model is the filled circle at a sediment density of zero. The model has a sedimentation rate of 2 m ka^{-1} and T_M of 748°C. Note the decrease in TNR with increasing sediment density. (b) Plot of time difference to narrow rifting (TDNR), calculated by subtracting the TNR of the model with sedimentation from that of its base model.

Figures 4 and 7 diverge. Shown at both the 5 and 12 Ma time slices, the sedimented model in example 2 (Figure 7) persists in wide rift mode. At low rates, sedimentation can increase the time needed to transition to a narrow rift, the opposite of what is observed at high sedimentation rates.

4. Model Discussion

[30] The calculations described here may have some bearing on the question of what processes lead to wide or narrow rifting. Sedimentation may affect the temperature structure of the crust by depressing isotherms, keeping the upper crust cool. This process would counter thermal advective weakening and promote wide rifting [*Sonder and England*, 1989]. It would also reduce thermal weakening at the rift edge, limiting the focusing of extension at the rift edge [*Huerta and Harry*, 2007]. *Huerta and Harry* [2007] used a half plateau model to demonstrate the focusing of extension at the plateau edge. In our full plateau model, this corresponds to the later stages of the wide rifting mode, with extension focused at both plateau edges. However, this prediction is the opposite of model behavior for all but the lowest sedimentation rates and counter to geological observations. This suggests that the temperature effect at reasonable sedimentation rates must be minimal compared to the effect of buoyancy forces. To understand which effects are controlling the behavior of these complex numerical models, it may be useful to consider analytic and semi-analytic treatments of component processes.

[31] In analyzing the model results we follow *Buck* [1991], who identified three main processes affecting continental extension: (1) advective thinning of crust and lithosphere (2) diffusion of heat, and (3) flow of lower crust. To these processes we add sedimentation. The processes are assumed to be important to the extent that they affect the tectonic force needed to continue extension. The most important components of that force are those relating to yield strength (F_{ys}), and crustal buoyancy (F_{cb}). In Appendix B we describe simple equations for the effect of extension and sedimentation on the crustal buoyancy force and yield strength. Here we neglect lower crustal flow since it is mainly important in allowing a ''core complex mode'' where the upper crust strains locally while the lower crust flows over a broad region. Here we are mainly concerned with the transition between wide and narrow rifting.

[32] Figure 8 shows two compilations of these forces for instantaneous thinning by a factor of $\varepsilon = 0.25$ for increasing amounts of sediment. Input values used are based on the initial setups from example 1 (Figure 8a) and a model with an initially cold Moho temperature. In the analytical treatment, the warmer system would not become a narrow rift until about 7 km of sediment is added. The numerical model roughly agrees with these numbers, as it starts as a wide rift, but with at least 8 km of sediment added, transitions to a narrow rift. The colder thermal regime (Figure 8b) never becomes a wide rift. Its evolution is dominated by the yield strength difference, and no reasonable amount of sediment alters its extensional mode. Similarly, numerical models colder than $T_M = 650$°C begin and persist as narrow rifts. No tested sedimentation rate altered that behavior (Figure 6).

Figure 4. (a) Initial crustal and thermal structure of model. Tabulation at top right gives values for the eight varied parameters. (b) Time slices at 2.5, 5, and 10.75 Ma for (left) the base model and (right) its corresponding sedimented model. At 2.5 Ma both models are passing through the core complex stage. The sedimented model has begun to accumulate a large volume of sediment in green. At 5 Ma the base model is in wide rifting mode, with two zones of major extension at the rift edges. In contrast, the model with sedimentation is in narrow rift mode, with extension located in one area through the entire section of lithosphere. It is not until 10.75 Ma that the base model is also in narrow rift mode. The sedimented model has persisted in narrow rift mode for this entire time. (c) Profile of the difference in temperature between the model with sedimentation and the base model at 5 Ma.

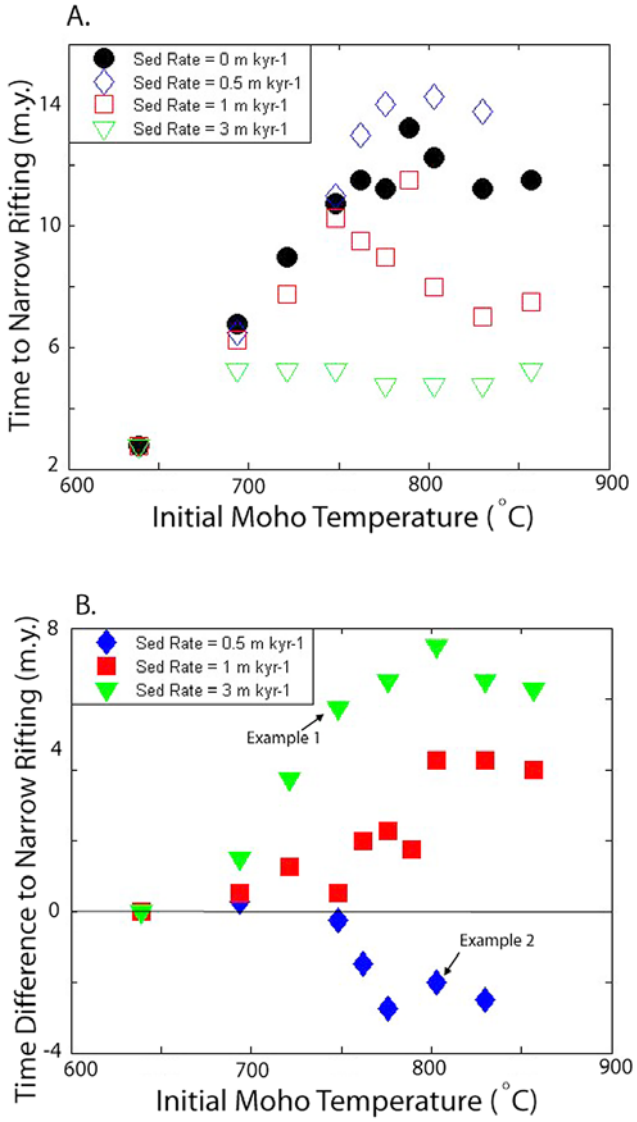

Figure 6. (a) Plot of TNR for series of models with sedimentation rates of 0.5 (open diamond), 1 (open square), and 3 (open triangle) m ka^{-1} and varied initial thermal conditions. The base model with a sedimentation rate of 0 m ka^{-1} is shown as the black circle. The general trend is a decreasing TNR with increasing sedimentation rate. Low sedimentation rates (here 0.5 m ka^{-1}) may show an increase in TNR due to the bulging effect discussed in the text. (b) Plot of TDNR derived from the plot in Figure 6a. Positive values indicate sediment caused an earlier transition to narrow rifting; negative values indicate a delayed transition. Examples 1 and 2 from Figures 4 and 7, respectively, are indicated.

[33] High yield strength leads to narrow rifting, while high crustal buoyancy leads to wide rifting. As initially hot, thick crust extends, it moves from core complex or wide rifting mode to narrow rifting due to crustal thinning [*Hopper and Buck*, 1996]. Sedimentation can affect this transition. The weight of added sediments reduces the crustal buoyancy force difference, forcing the system to a narrow rift mode sooner (Figure 1).

[34] As mentioned above, the addition of cold sediment can also depress isotherms. Such an effect is not treated in our analytical model but would create a colder thermal profile, reducing the yield strength difference, and aide wide rifting. However, as our analytical model agrees with our numerical model which includes such an effect, we predict this effect to be negligible.

[35] If buoyancy forces are a controlling factor in determining extensional mode, then increasing sediment load should decrease the buoyancy force difference and produce an earlier transition to narrow rifting. This prediction matches the observed relationship between sediment density and TDNR shown in Figure 5. The heavier the load, the more the crust is depressed, decreasing the force difference. Increased sedimentation rate would also increase the sediment load during rifting, and as predicted, models with higher sedimentation rates transition to narrow rifting quicker then their base models (Figure 6).

[36] *Lizarralde et al.* [2007] suggested that large inputs of sediment may have a thermal blanketing effect, where the continental crust is heated by being depressed to deeper isotherms, thereby weakening it. Presumably, thermal blanketing would promote narrow rifting in the area of thickest sediments. However, in the numerical models presented here, narrow rifting initiates toward the sides of the rift, but not in the middle of the thinned area, where the thickest sediments would be accumulated. This occurs because the main thermal effect of sediment addition at a moderately high rate is to push isotherms down, thus, thickening and strengthening the lithosphere, similar to the semianalytical results or because the thermal effect is negligible compared to the buoyancy effect.

[37] *Huerta and Harry* [2007] have suggested that thermal weakening at the rift edge plays a major role in focusing extension from wide to narrow at the rift edge. We agree that this is the case when no sediment is involved, but thermal weakening does not have a major influence with substantial sedimentation. At low sedimentation rates (Figures 6 and 7) sedimentation actually increases the time in wide rift mode. In the wide rift stage as simulated here, the zone of crustal thinning migrates from the more central parts of the plateau toward the edges, similar to the results of *Huerta and Harry* [2007]. For models with low sedimentation rates, such as example 2, the edges have not been at low enough elevation to accumulate a significant sediment cover while the center of the thinned area continues to accumulate sediment (Figure 7). Isotherms are depressed in the more sedimented central areas of the former plateau, strengthening the crust, but the zone of active rifting, now focused at the two plateau edges, remains hot and weak as predicted by *Huerta and Harry* [2007] (Figure 7c). In contrast, both the center and the edges of the thinned area in example 1 have depressed isotherms at the time the sedimented model transitions to narrow rifting (Figure 4c). The hotter the initial thermal conditions, the higher the sedimentation rate must be to counter this effect (Figure 6).

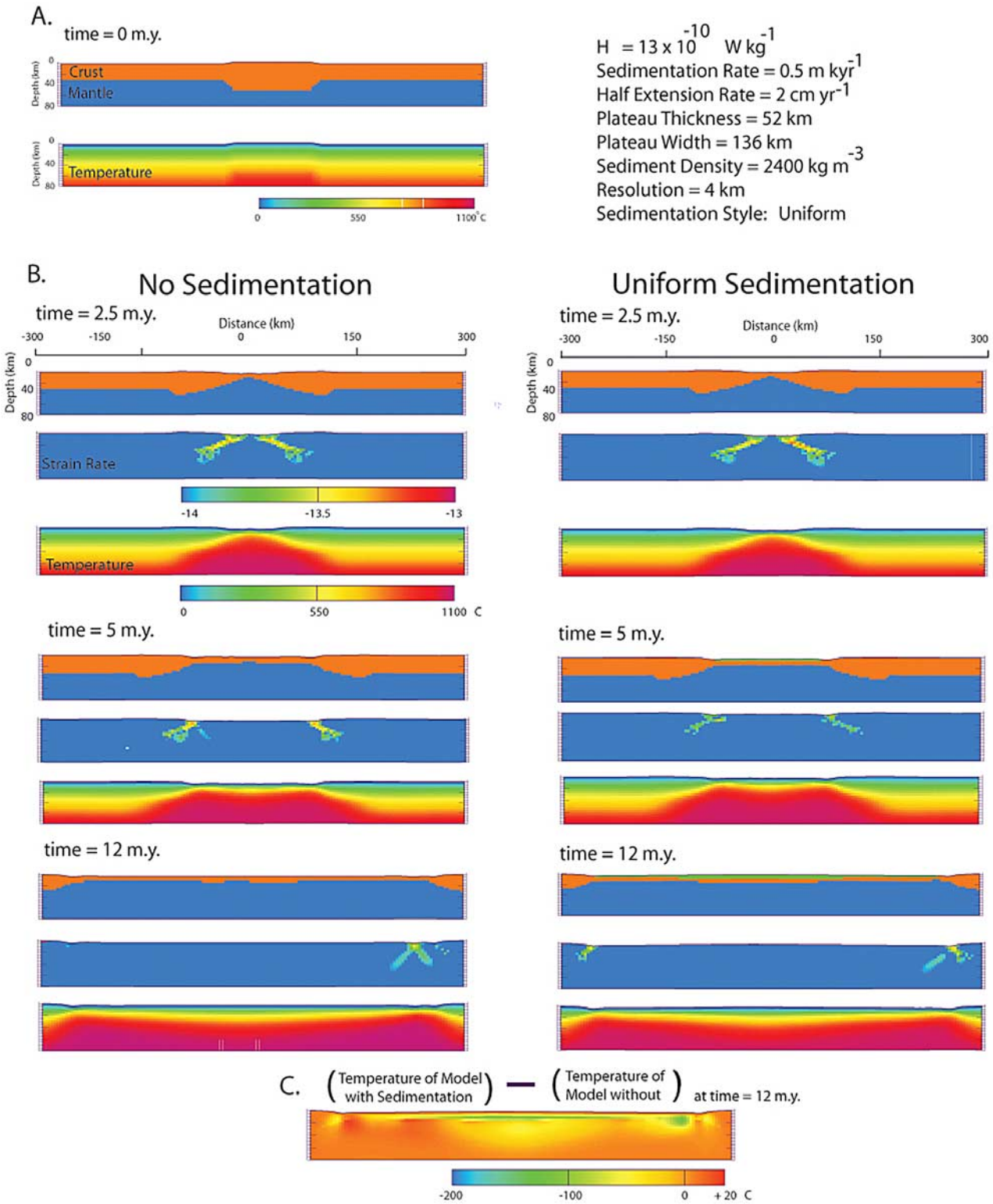
A.
time = 0 m.y.
Crust
Mantle
Temperature
0
550
1100°C
H = 13 x 10^-10 W kg^-1
Sedimentation Rate = 0.5 m kyr^-1
Half Extension Rate = 2 cm yr^-1
Plateau Thickness = 52 km
Plateau Width = 136 km
Sediment Density = 2400 kg m^-3
Resolution = 4 km
Sedimentation Style: Uniform
B.
No Sedimentation
Uniform Sedimentation
time = 2.5 m.y.
Distance (km)
-300
-150
0
150
300
Depth (km)
Strain Rate
-14
-13.5
-13
Temperature
0
550
1100 C
time = 5 m.y.
time = 12 m.y.
C.
(Temperature of Model with Sedimentation) — (Temperature of Model without) at time = 12 m.y.
-200
-100
0
+20 C

Figure 7

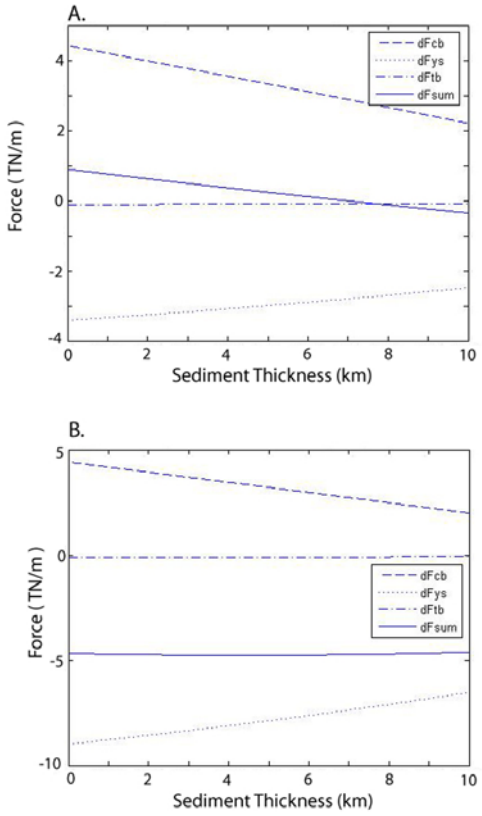

Figure 8. Two examples of 1-D calculations using values listed in Table B1. Crustal buoyancy force difference, dF_{cb}; yield strength force difference, dF_{ys}; thermal buoyancy force difference, dF_{tb}; summary of forces, dF_{Sum}. (a) Increasing sediment load decreases the crustal buoyancy force difference at a fast rate than yield strength force difference. This example would extend as a wide rift unless ~7 km of sediment is added. (b) In this colder example, the buoyancy force difference decrease is matched by the change in the yield strength force decrease. The model would extend as a narrow rift and is not affected by sedimentation.

[38] The thermal effect associated with low sedimentation rates in our models may not be realistic. Sediment continues to be deposited in the middle of a rift with a greater elevation (due to the sediment history) at the same rate as zones of high strain. We know of no example in nature where the center of a rift has such a sediment bulge. We therefore concern ourselves with the more realistic higher sedimentation rate.

5. Gulf of California

[39] The Gulf of California may be an extended region where sedimentation changed the style of rifting. Recent seismic results for the Gulf of California clearly show a difference in extensional style from north to south within the rift [*Lizarralde et al.*, 2007]. The heavily sedimented northern (Figure 9, Delfin-Tiburon) [*González-Fernández et al.*, 2005] and north central gulf (Figure 9, Yaqui and Guaymas segment) [*Aragón-Arreola et al.*, 2005; *Lizarralde et al.*, 2007] exhibit a quick transition from wide rifting to narrow rifting as compared to the sediment starved southern gulf (Alarcon segment) [*Lizarralde et al.*, 2007]. However, the southernmost gulf (Cabo-PV segment), also sediment starved, appears to have become a narrow rift earlier in its development. We agree with the interpretation that this transition was influenced by proximity to the East Pacific Rise, perhaps due to lateral supply of magma [*Lizarralde et al.*, 2007]. Our models of sedimented versus sediment starved rifts may provide insight into the development of the difference between the northern and central gulf basins.

5.1. Regional Tectonic and Depositional History

[40] The western edge of Baja was a site of active subduction of the Farallon plate under the North American plate from the late Mesozoic into the Miocene. The transition from subduction to a transform boundary was accommodated by the northward and southward migration of two triple junctions [*Atwater and Molnar*, 1973]. During the later stages of subduction, Basin and Range style extension migrated southward into the Gulf Extensional Province (Figure 9) [*Henry and Aranda-Gomez*, 1992]. East-northeast opening was accommodated on N-S orientated grabens beginning around 16 Ma [e.g., *Lee et al.*, 1996]. Alternatively, the period of extension from 16 to 12 Ma may have been the result of back-arc spreading [*Karig and Jensky*, 1972].

[41] At ~12 Ma, subduction ceased and the Guadalupe and Magdalena microplates were captured by the Pacific plate. The motion between the Pacific and North American plate may have been split into right lateral, NW motion and NE-SW half graben extension during the protogulf stage [*Stock and Hodges*, 1989]. A 6.5 Ma marine incursion at Isla Tiburón, which corresponds to marine deposits in the

Figure 7. (a) Initial crustal and thermal structure of model example 2. Tabulation at top right gives values for the eight varied parameters. (b) Time slices at 2.5, 5, and 12 Ma for (left) the base model and (right) its corresponding sedimented model. At 2.5 Ma both models are passing through the core complex stage. At 5 Ma both models are in wide rifting mode. The model with sedimentation has accumulated a thin veneer of sediments. At 12 Ma the base model has almost completely transitioned to a narrow rift. The model with sedimentation, in contrast, is still fully in wide rifting mode. A bulge of sediments has developed with a very thick sediment pile in the middle of the extended domain and little to no sediment at the sites of active rifting. (c) Profile of the difference in temperature between the model with sedimentation and the base model at 12 Ma, when at least the base model has begun the transition to narrow rifting. Note that both rift edges are hotter in the sedimented model than the base model.

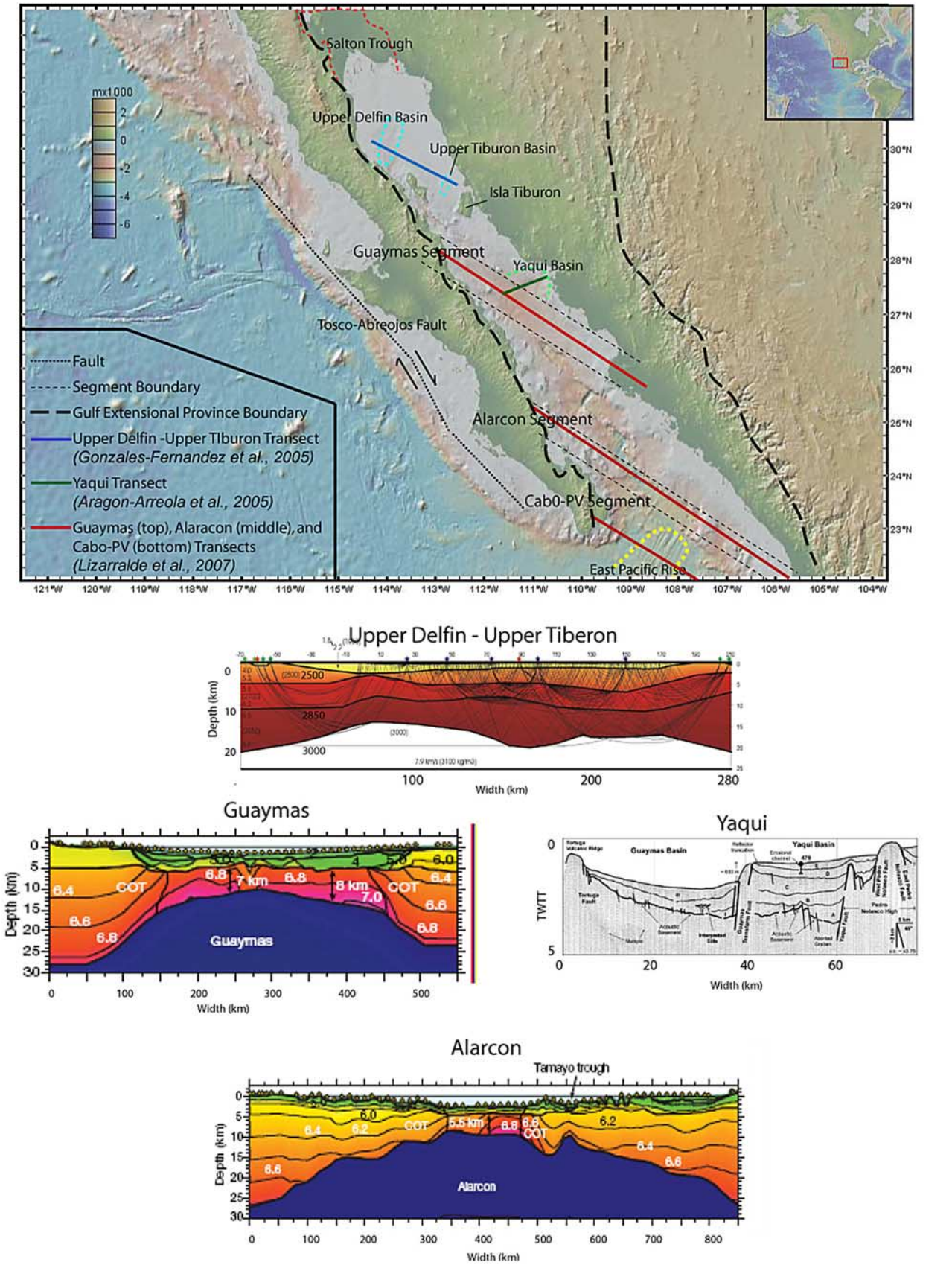
Salton Trough
Upper Delfin Basin
Upper Tiburon Basin
Isla Tiburon
Guaymas Segment
Yaqui Basin
Tosco-Abreojos Fault
Alarcon Segment
Cab0-PV Segment
East Pacific Rise
mx1000
Fault
Segment Boundary
Gulf Extensional Province Boundary
Upper Delfin -Upper TIburon Transect
(Gonzales-Fernandez et al., 2005)
Yaqui Transect
(Aragon-Arreola et al., 2005)
Guaymas (top), Alaracon (middle), and
Cabo-PV (bottom) Transects
(Lizarralde et al., 2007)
Upper Delfin - Upper Tiberon
Depth (km)
Width (km)
Guaymas
COT
Guaymas
Yaqui
Guaymas Basin
Yaqui Basin
TWTT
Width (km)
Alarcon
Tamayo trough
Alarcon
Depth (km)
Width (km)

Figure 9

Salton Trough [*McDougall et al.*, 1999; *Dorsey et al.*, 2007], has been interpreted to coincide with the transfer of Baja to the Pacific plate [*Oskin and Stock*, 2003]. This transfer marks the end of the protogulf stage and the establishment of the current transtentional regime in the Gulf of California.

[42] The earliest sediments of the Colorado River recorded at Split Mountain Gorge in the Salton Trough appear via north to south transport at 5.3 Ma [*Dorsey et al.*, 2007]. Rapid initiation of the Colorado River [*Dorsey et al.*, 2007, and references therein] would have delivered large amounts of sediment to the gulf region early in the river's development. Modern sedimentation rates in upper Delfín and upper Tiburón are on the order of $\sim$3 m ka^{-1} [*Van Andel*, 1964], with large amounts of terrigenous material from the Colorado River.

5.2. Tectonic, Depositional, and Magmatic History of Focus Areas

[43] In the northern Gulf of California, the Delfín and Tiburón basins (Figure 9) show evidence of only minimal dextral displacement prior to $\sim$6.3 Ma and 255 km after the plate reorganization [*González-Fernández et al.*, 2005]. Since 6.3 Ma, the northern gulf shows an evolution of focused core complex rifting and wide rifting in the upper Tiburón basin to narrow rifting in the upper Delfín basin [*González-Fernández et al.*, 2005]. A maximum of 100 km of slip is reported for the Tiburón basin, thinning the crust from 30 km to less than 19 km. At $\sim$3 Ma, extension jumped to the Delfín basin where it progressed to narrow rifting with some magmatism. Sediment thickness along this transect is at a maximum of 7 km in the Upper Tiburón basin [*González-Fernández et al.*, 2005]. Distributed, recent normal faulting in the top 1 km of sediment is observed in the Delfin basin [*Persaud et al.*, 2003].

[44] Moving south along the gulf, the Guaymas basin (Figure 9) represents the last of the heavily sedimented northern basins and the first basin of the central domain, located south of a kink in the obliquity of extension below which extension is more parallel to the relative plate motion [*Axen et al.*, 2006]. The Guaymas segment shows evidence of 70 km of extension before the onset of crustal accretion at $\sim$6 Ma, which accommodates $\sim$280 km of extension [*Lizarralde et al.*, 2007]. Up to 5 km of sediments and intrusives are interpreted to lie above the new crustal material in the Guaymas basin. This extension total neglects protogulf extension in the adjacent Yaqui basin (Figure 9) [*Aragón-Arreola et al.*, 2005] and likely extension in the Sonora coast. The Yaqui basin contains 4–5 km of wedge fill sediments with projected dates from the Late Miocene to Pleistocene boundary [*Aragón-Arreola et al.*, 2005].

[45] In contrast to the Guaymas-Yaqui and Delfin-Tiburón segments, the Alarcon segment (Figure 9) exhibits wide rift characteristics for a much longer period time [*Lizarralde et al.*, 2007]. Multiple areas of mantle necking are interpreted and the crust is thinned over a much wider area. About 350 km of extension is reported prior to the onset of seafloor spreading with an additional $\sim$135 km of new 6 km thick crust added since the transition to seafloor spreading at about 3.6 Ma [*Lizarralde et al.*, 2007]. There are less than 1 km of sediments and synrift magmatism in the Alarcon segment.

6. Application of Model Results to Observations

[46] It is important to note that these models test a concept, but cannot portray all idiosyncrasies of the Gulf of California or any real rift system. Though an effort is made to match some of the geological constraints, such as total extension, velocity, and crustal structure, models cannot replicate everything observed. Our model does not include hydrothermal cooling [*Lavier and Buck*, 2002] or any other strengthening feature, such as strain hardening [*Sonder and England*, 1989], that would counter thermal advective weakening and might lead to more evenly distributed extension in the upper crust. As a result, the wide mode includes only two major zones of extension near the plateau edges.

[47] We plan to include this fairly complex effect in future models, but expect that sediment will still hasten the transition to narrow rifting for most model situations.

[48] In addition, a 3-D code would be needed to model the strike-slip component of extension and to truly model transtension. However, for the Gulf of California, the most significant strike slip extension occurs during the protogulf period, during which there is no known large input of far-field sediment. Other complications, such as the influence of slab window tectonics and upwelling aesthenosphere after subduction ceases could influence the extension regime and are not taking into account here. Despite these limitations, we believe the large-scale processes driving both the Gulf of California and our models to be the same. The numerical models presented here do demonstrate that sedimentation can lead to a faster transition to narrow rifting.

6.1. Application to Gulf of California Focus Areas

6.1.1. Tectonic Timing and Sediment Distribution

[49] Just as in the models, regions of the gulf with thick sediment cover (Delfín-Tiburón and Guaymas-Yaqui) transition to narrow rifting faster than sediment poor regions

Figure 9. Map of the Gulf of California with four recent seismic profiles from three different experiments shown at bottom. Note the different horizontal and vertical scales between transects. The blue transect presents a velocity model of the Upper Delfin and Upper Tiburon basins from multichannel seismic reflection and seismic refraction data [*González-Fernández et al.*, 2005]. The green transect is a multichannel seismic reflection survey across the Yaqui and Guaymas basins [*Aragón-Arreola et al.*, 2005]. The red transects are velocity models of the Guaymas and Alarcon segments from seismic refraction data [*Lizarralde et al.*, 2007].

(Alarcon). The Delfin-Tiburon segment shows evidence of minor extension in the protogulf period, core complex and wide characteristics from 6.3 to 3 Ma, and narrow rifting from 3 Ma to present. The Guaymas segment transitioned to narrow rifting after at least 70 km opening at 6 Ma and has been narrow since. The Alarcon segment extended under wide conditions during the protogulf period and into the transtensional period for 350 km before transitioning to narrow rifting at 3.6 Ma, which is 2.4 Ma and 135 km longer than the Guaymas segment.

[50] The key difference between the basins is the presence of up to 7 km of sediment in the Tiburon-Delfin segment, ~5 km of sediments in the Guaymas basin and neighboring Yaqui basin, compared to negligible sediment cover in the Alarcon segment. This is similar to our model results, where models with thick sediment cover transition to narrow rifts earlier than a corresponding model with little to no sedimentation (Figure 4). Despite the many complexities associated with 3-D effects of transtention, our model results agree with the geographic location and timing of the onset of narrow rifting.

6.1.2. Sediment Timing

[51] The timing of the sediments compared to the timing of narrow rifting is central to our concept. The Tiburon-Delfin segments transitioned to narrow rifting at ~3 Ma [*González-Fernández et al.*, 2005], after the initiation of the Colorado River at 5.3 Ma [*Dorsey et al.*, 2007]. Sediments in the Yaqui basin are reported as late Miocene to late Pliocene, whereas basal sediments in the Guaymas basin are projected to be from the Pliocene [*Aragón-Arreola et al.*, 2005]. The exact dates of these sediments are unknown.

[52] Our conceptual model agrees with the timing of sedimentation in the northern gulf, but is problematic in the north central gulf. *Lizarralde et al.* [2007] reports that narrow rifting began at ~6 Ma in the Guaymas basin, too early for Colorado River sediments (~5.3 Ma) to influence the mode of extension. For our conceptual model for the Gulf of California to be applicable in north central gulf, either large amounts of sediment began accumulating in the Yaqui and Guaymas basins before Colorado River initiation, the Guaymas basin is the last basin to feel the buoyancy effects of the large sediment load in the north, or the *Lizarralde et al.* [2007] model overinterprets the extent of new oceanic crust. If as little as 20–40 km of what *Lizarralde et al.* [2007] consider igneous crust is in fact continental crust altered or intruded by sills and dikes, then the timing of extension versus Colorado River initiation would be in agreement with our model.

6.1.3. Sediment Thickness

[53] The sediment thickness of the model in example 1 (Figure 4) exceeds that observed in the Gulf of California. To create a more realistic simulation, we alter the sediment delivery algorithm to deposit sediment only in the deepest area of the rift. Using this focused sedimentation scenario, more realistic sediment thicknesses can produce similar results (Figure 10), without creating the bulge effect shown in Figure 7 and discussed earlier. This focused sedimentation approach delivers sediment to the most active part of the rift, decreasing the buoyancy force difference where it would have the largest effect. The two sediment deposition rules used in this study are not comprehensive nor do they mimic a true surface processes model. They do, however, successfully test our concept of whether sediment can influence extensional style by affecting the buoyancy forces.

6.2. Other Examples

[54] The Gulf of Lion in the northern Mediterranean may be another example of deposition of sediment sourced far from the rift influencing the extensional style. The magnitude of subsidence and sediment thickness in the Gulf of Lion is too large compared with the amount of observed extension [*Steckler and Watts*, 1980]. Segmentation of the rift corresponds to varying amounts of subsidence [*Berne and Gorini*, 2005]. Most of these sediments are postrift in the Gulf of Lion [*Steckler and Watts*, 1980], but their timing corresponds with the opening of the adjacent Ligurian Sea [*Rollet et al.*, 2002]. Though not explored thoroughly here, the Gulf of Lion and Ligurian Sea may be another example of sediment influencing the extensional mode and is an excellent candidate for future work.

7. Conclusions

[55] Sedimentation derived from a far field source deposited during rifting can influence the extensional mode of the rift. Sedimentation reduces the crustal buoyancy force difference, leading to conditions more conducive to narrow rifting. Increasing sediment load, achieved through higher sedimentation rates or higher sediment density, decreases the buoyancy force difference and decreases the total time needed to transition to a narrow rift. In the numerical wide rift mode, sediments must accumulate in the zones of active rifting in order to affect the buoyancy forces.

[56] The deposition of sediment also affects the thermal structure of the system by depressing isotherms. In unsedimented models, the transition from wide to narrow rifting is in part controlled by thermal weakening of the crust at the rift edges [*Huerta and Harry*, 2007]. When sediment is deposited at these rift edges, isotherms are depressed, and this thermal affect is reduced. However, our numerical sedimented models transition to a narrow rift earlier those without sediment, demonstrating the importance of buoyancy forces over thermal forces when sedimentation is active. We agree with *Lizarralde et al.*'s [2007] statement that the crystalline continental crust now under the sediment would be hotter and weaker, but the location of the narrow rift does not correspond with the greatest sediment levels, arguing against thermal blanketing controlling the transition to narrow rifting.

[57] The Gulf of California may be an area where sedimentation from a distant source has influenced the extensional style. The northern (Delfin-Tiburon segment) and north central Gulf (Guaymas-Yaqui segment), with thick sediment cover, transitioned to narrow rifting several million years earlier into their development than the sediment starved south central Gulf (Alarcon segment). The timing of the transition to narrow rifting in the gulf and the

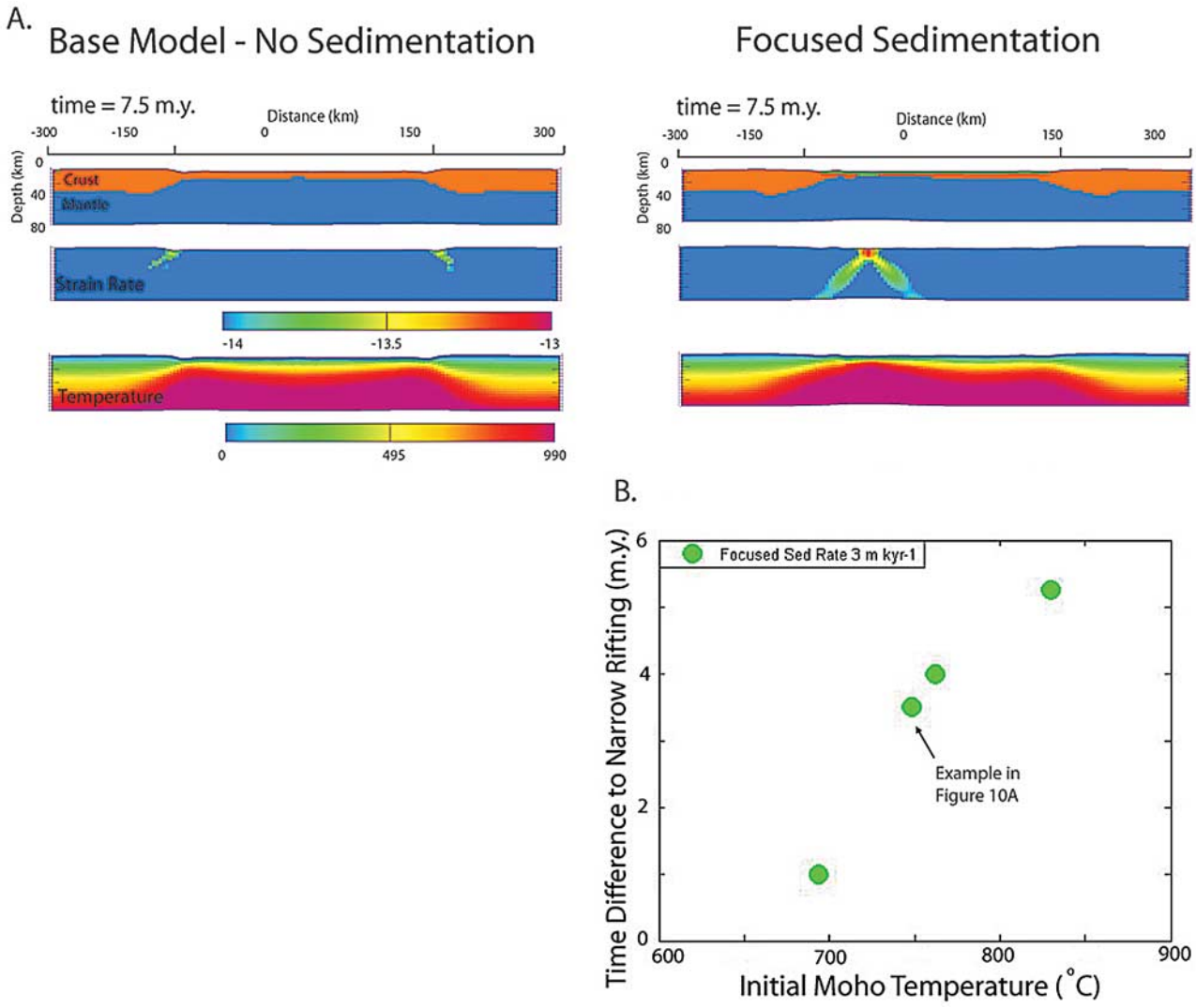

Figure 10. (a) The 7.5 Ma time slice from a base model and model with focused sedimentation. Other model parameters are the same as example 1 in Figure 4. The model with focused sedimentation algorithm is able to transition to narrow rifting at 7.5 Ma while the corresponding base model persists as a wide rift until 10.75 Ma. The model with focused sedimentation has only 4–8 km of sediments in the rifted area. (b) TDNR is shown for a series with a focused sedimentation rate of 3 m ka^{-1} and varied initial thermal conditions. Result is similar to that of the uniform sedimentation algorithm shown in Figure 6, but less total sediment is required.

distribution of sediment agree with our model results, although with some possible discrepancy in the Guaymas segment. The influence of the sediment appears to be the major factor differentiating extensional history of the northern Gulf from the south.

Appendix A: Numerical Model

[58] Deformation is tracked using an explicit finite element method similar to the FLAC (fast Lagrangian analysis of continua) technique [*Lavier et al.*, 2000; *Cundall*, 1989, and references therein]. It has been used to investigate local deformation [e.g., *Buck and Polikov*, 1998; *Lavier et al.*, 2000, and references therein] and regional deformation [*Buck et al.*, 1999, 2001; *Bialas et al.*, 2007].

[59] At each time step, Newton's second law is solved at every grid point. The forces present at each grid point are summed, and the "out-of-balance" forces and the mass at the grid point are used to calculate the acceleration. The accelerations are integrated to calculate the velocities which are used to determine the increment of strain at each grid point. Using Mohr-Coulomb criterion for plasticity and Maxwell's criterion viscoelasticity, the corresponding stress increments and the forces they produce on the surrounding grid points are summed to determine the new out-of-balance forces. The effects of inertia are damped in order to approximate quasi-static processes.

Table B1. Analytical Variables[a]

Parameter	Definition	Value in Figure 8a	Value in Figure 8b
ε	strain	0.25	0.25
g	gravity (m s^{-2})	9.8	9.8
ρ_m	mantle density (kg m^{-3})	3300	3300
ρ_s	sediment density (kg m^{-3})	2400	2400
ρ_c	crustal density (kg m^{-3})	2800	2800
h	crustal thickness (km)	52	52
h_s	sediment thickness (m)	varied	varied
α	thermal expansion coefficient (K^{-1})	3×10^{-5}	3×10^{-5}
T_m	Moho temperature (K)	800	600
T_s	surface temperature (K)	0	0
Z_m	depth of mantle brittle-ductile transition (km)	52	56
Z_c	depth of crustal brittle-ductile transition (km)	30	44
gB	pressure gradient (Pa m^{-1})	12,000	12,000
$\dot{\varepsilon}$	strain rate (s^{-1})	1×10^{-14}	1×10^{-14}
X_e	width of initially uniform lithosphere (km)	50	50
X_L	width of extension zone (km)	100	100
κ_f	thermal diffusivity (m^2 s^{-1})	1×10^{-6}	1×10^{-6}

[a]Derived terms are $\Delta\rho^* = \rho_c\ (\rho_m - \rho_c)/\rho_m$(kg m^{-3}) and $\Delta\rho_s^* = [(h\varepsilon/(h\varepsilon + h_s)) * \Delta\rho^*] + [(h_s/(h\varepsilon + h_s)) * (\rho_s(\rho_m - \rho_s)/\rho_m)]$. Assuming no lower crustal flow, $F(\kappa_f, \dot{\varepsilon}) = \mathrm{erf}(X_e/4\sqrt{\kappa_f\varepsilon/\dot{\varepsilon}}) - \frac{1}{2}\mathrm{erf}((X_e + X_L)/4\sqrt{\kappa_f\varepsilon/\dot{\varepsilon}}) - \frac{1}{2}\mathrm{erf}((X_e - X_L)/4\sqrt{\kappa_f\varepsilon/\dot{\varepsilon}}) = 1$.

[60] For our model parameters, the time step in this explicit time-marching scheme is governed by the elastic properties. We increase the speed of calculations by setting the boundary displacement as a fraction of grid spacing per time step. To set the boundary displacement, we chose a ratio of boundary velocity to sound velocity of 5×10^{-5}. We find this ratio allows for fast runs while minimizing the error on the strain calculation. Typically, time steps are on the order of 3 to 6 years.

[61] The initial mesh of the model is made of quadrilaterals subdivided into two pairs of superimposed constant strain triangular zones. Since the method is Lagrangian, i.e., the numerical grid follows the deformation, the simulation of very large deformation involves remeshing to overcome the problem of degradation of numerical precision when elements are distorted. We trigger remeshing when one of the triangles in the grid elements is distorted below a critical angle, set to 20°. With remeshing, strains at each grid point are interpolated between the old deformed mesh and the new undeformed mesh using a linear interpolation algorithm. The new state of strain is used with the rheological laws to calculate the stress and resulting out-of-balance forces to start the time step cycle again. The element phases, representing the sediment, diabase or olivine rheology, are treated similarly during remeshing. New material with the same properties as the bottom mantle layer is added to replace lithosphere that is pulled out of the sides of the model box.

[62] The brittle strength of the lithosphere is assumed to be limited by Mohr-Coloumb yielding with a friction coefficient of 0.6 and an initial cohesion of 44 MPa. Strain weakening is applied in the model [*Lavier et al.*, 2000]. Between plastic strain values of 0 to 1.2, the cohesion decreases linearly from 44 to 4 MPa. The temperature-dependent viscous rheology of the crust is based on a creep flow power law for diabase, and the mantle has an olivine rheology [*Kirby and Kronenberg*, 1987].

[63] Advection and diffusion of heat are tracked since temperature changes affect rheology. Initial temperature profiles are calculated using conductive heat transport assuming that radiogenic heat production in the crust decreases exponentially with depth as $H = H_0 e^{-y/h_r}$, where H is the concentration of radiogenic elements, y is depth, and h_r is 10 km [*Turcotte and Schubert*, 2002]. The concentration of radiogenic elements at the surface, H_0, was varied from 0 to 8.6 μW m^{-3}, similar to the results of *Bialas et al.* [2007].

[64] The initial temperature is set to the initial 1-D steady state value using

$$T = T_0 + \frac{q_m z}{k} + \frac{\rho H_0 h_r^2}{k}\left(1 - e^{-z/h_r}\right)$$

where T is the temperature, T_0 is the surface temperature set to 0°C, k_c is crustal thermal conductivity set to 2.5 W m^{-1} K^{-1}, k_m is mantle thermal conductivity set at 3.3 W m^{-1} K^{-1}, q_m is the mantle heat flux set at 0.029 W m^{-2}, ρ is the density, and z is depth [*Turcotte and Schubert*, 2002]. The temperature at the base of the model is set to the initial temperature of the bottom element under the base of the plateau. Tests using an initial 2-D steady state temperature structures, calculated by letting the model run without extension until a steady state temperature is achieved, have little effect on model results.

[65] In most models, grid spacing is about 4 km. This spacing allows models to be completed in a reasonable amount of time while still allowing enough detail to examine regional features. Model runs with a finer mesh using 2 km grid spacing take ~8 times longer to complete but produce similar results. Tests showed similar patterns, so a 4 km grid spacing was used in order to perform a large number of experimental runs.

Appendix B: Effect of Extension and Sedimentation on Crustal Buoyancy and Yield

[66] The change crustal buoyancy force, dF_{cb}, is described as $dF_{cb} = [1 - \exp(-\varepsilon)](g\Delta\rho^* h^2)$ when lower crustal flow is assumed to be negligible (see Table B1 for variables). Large, positive dF_{cb} forces the system to rift in wide mode, and negative values lead to narrow rifting. By adding sedimentation, we effectively thicken the crust, which reduces dF_{cb} as $dF_{cb} = [(g\Delta\rho^* h^2)] - \{[\exp[-(\varepsilon - (h_s/h))]]^*(g\Delta\rho_s^* h^2)\}$. Reducing dF_{cb} forces the system closer to the narrow rifting mode [*Buck*, 1991].

[67] Sedimentation may also affect the strength and temperature profiles within the lithosphere. Without sedimentation, strong upper mantle replaces the lower and middle crust in highly thinned areas, and areas of high strain rates persist at the edges of the rift. With sedimentation, weaker crustal rocks remain present at midcrustal levels, and extension can continue at the same site for longer.

[68] The yield strength difference,

$$dF_{ys} = -\{1 - \{\exp[-[2(\varepsilon - (h_s/h))]]\}\}\left(\frac{gB}{2}\right)\left[Z_c^2 + Z_m^2 - h^2\right],$$

and thermal buoyancy difference,

$$dF_{tb} = -\{1 - \{\exp[-[2(\varepsilon - (h_s/h))]]\}\}\left(\frac{g\alpha\rho_m(T_m - T_s)Z_m^2}{6}\right),$$

are affected by the addition of sediment by reducing the thinning factor, ε, by h_s/h, as in dF_{cb}. The result is an increase in dF_{ys} toward positive, wide rifting values.

[69] **Acknowledgments.** We would like to thank NSF EAR 04-09287 for funding this work; Todd Ehlers, Audrey Huerta, and an anonymous reviewer for their thoughtful reviews; and Dan Lizarralde for helpful discussions.

References

Aragón-Arreola, M., M. Morandi, A. Martín-Barajas, L. Delgado-Argote, and A. González-Fernández (2005), Structure of the rift basins in the central Gulf of California: Kinematic implications for oblique rifting, *Tectonophysics*, *409*, 19–38, doi:10.1016/j.tecto.2005.08.002.

Atwater, T. M., and P. Molnar (1973), Relative motion of the Pacific and North American plates deduced from sea-floor spreading in the Atlantic, Indian, and South Pacific oceans, in *Proceedings of the Conference on Tectonic Problems of the San Andreas Fault System*, edited by R. Kovach and A. Nur, *Stanford Univ. Publ. Geol. Sci.*, *16*, 136–148.

Avouac, J. P., and E. B. Burov (1996), Erosion as a driving mechanism of intracontinental mountain growth, *J. Geophys. Res.*, *101*, 17,747–17,769, doi:10.1029/96JB01344.

Axen, G., A. Stelly, S. Janecke, M. Kairouz, N. Black, C. Shirvell, and B. Housen (2006), Low-angle normal faults in the northern gulf: Summary and implications for fault mechanics and strain partitioning, paper presented at RCL-Cortez MARGINS Workshop, NSF-MARGINS Program, Ensenada, Mexico, 9–13 Jan.

Bassi, G., C. E. Keen, and P. Potter (1993), Contrasting styles of rifting: Models and examples from the eastern Canadian margin, *Tectonics*, *12*, 639–655, doi:10.1029/93TC00197.

Beaumont, C., R. A. Jamieson, M. H. Nguyen, and S. Medvedev (2004), Crustal channel flows: 1. Numerical models with applications to the tectonics of the Himalayan-Tibetan orogen, *J. Geophys. Res.*, *109*, B06406, doi:10.1029/2003JB002809.

Berne, S., and C. Gorini (2005), The Gulf of Lion: An overview of recent studies with the French 'Margins' programme, *Mar. Pet. Geol.*, *22*, 691–693, doi:10.1016/j.marpetgeo.2005.04.004.

Bialas, R. W., W. R. Buck, M. Studinger, and P. G. Fitzgerald (2007), Plateau collapse model for the Transantarctic Mountains–West Antarctic Rift System: Insights from numerical experiments, *Geology*, *35*, 687–690, doi:10.1130/G23825A.1.

Brace, W. F., and D. L. Kohlstedt (1980), Limits on lithospheric stress imposed by laboratory experiments, *J. Geophys. Res.*, *85*, 6248–6252, doi:10.1029/JB085iB11p06248.

Buck, W. R. (1991), Modes of continental lithospheric extension, *J. Geophys. Res.*, *96*, 20,161–20,178, doi:10.1029/91JB01485.

Buck, W. R., and L. L. Lavier (2001), A tale of two kinds of normal fault: The importance of strain weakening in fault development, in *Non-volcanic Rifting of Continental Margins: A Comparison of Evidence From Land and Sea*, edited by R. C. L. Wilson et al., *Geol. Soc. Spec. Publ.*, *187*, 340–355.

Buck, W. R., and A. N. B. Polikov (1998), Abyssal hills formed by stretching oceanic lithosphere, *Nature*, *392*, 272–275, doi:10.1038/32636.

Buck, W. R., L. L. Lavier, and A. N. B. Poliakov (1999), How to make a rift wide, *Philos. Trans. R. Soc. London*, *357*, 671–693, doi:10.1098/rsta.1999.0348.

Burov, E., and A. Poliakov (2001), Erosion and rheology controls on synrift and postrift evolution: Verifying old and new ideas using a fully coupled numerical model, *J. Geophys. Res.*, *106*, 16,461–16,481, doi:10.1029/2001JB000433.

Cundall, P. A. (1989), Numerical experiments on localization in frictional materials, *Arch. Appl. Mech.*, *59*, 148–159, doi:10.1007/BF00538368.

Dewey, J. F., and A. M. C. Segnor (1979), Aegean and surrounding regions: Complex multiplate and continuous continuum tectonics in a convergence zone, *Geol. Soc. Am. Bull.*, *90*, 84–92, doi:10.1130/0016-7606(1979)90<84:AASRCM>2.0.CO;2.

Dorsey, R. J., A. Fluetta, K. McDogall, B. A. Housen, S. U. Janecke, G. J. Axen, and C. R. Shirvell (2007), Chronology of Miocene-Pliocene deposits at Split Mountain Gorge, southern California: A record of regional tectonics and Colorado River evolution, *Geology*, *35*, 57–60, doi:10.1130/G23139A.1.

England, P. (1983), Constraints on Extension of Continental Lithosphere, *J. Geophys. Res.*, *88*, 1145–1152, doi:10.1029/JB088iB02p01145.

González-Fernández, A., J. J. Dañobeitia, L. A. Delgado-Argote, F. Michaud, D. Córdoba, and R. Bartolomé (2005), Mode of extension and rifting history of upper Tiburón and upper Delfín basins, northern Gulf of California, *J. Geophys. Res.*, *110*, B01313, doi:10.1029/2003JB002941.

Goodge, J. W. (2002), From Rodinia to Gondwana: Supercontinent evolution in the Transantarctic Mountains, in *Antarctica at the Close of a Millennium*, edited by J. A. Gamble, D. N. B. Skinner, and S. Henrys, *Bull. R. Soc. N. Z.*, *35*, 61–74.

Hamilton, W. B. (1987), Crustal extension in the Basin and Range province, southwestern United States, in *Continental Extensional Tectonics*, edited by M. P. Coward, J. F. Dewey, and P. L. Hancock, *Geol. Soc. Spec. Publ.*, *28*, 155–176.

Harry, D. L., D. S. Sawyer, and W. P. Leeman (1993), The mechanics of continental extension in western North America: Implications for the magmatic and structural evolution of the Great Basin, *Earth Planet. Sci. Lett.*, *117*, 59–71, doi:10.1016/0012-821X(93)90117-R.

Henry, C. D., and J. J. Aranda-Gomez (1992), The real southern Basin and Range: Mid- to late Cenozoic extension in Mexico, *Geology*, *20*, 701–704, doi:10.1130/0091-7613(1992)020<0701:TRSBAR>2.3.CO;2.

Hopper, J. R., and W. R. Buck (1996), The effect of lower crustal flow on continental extension and passive margin formation, *J. Geophys. Res.*, *101*, 20,175–20,194, doi:10.1029/96JB01644.

Huerta, A. D., and D. L. Harry (2007), The transition from diffuse to focused extension: Modeled evolution of the West Antarctic Rift System, *Earth Planet. Sci. Lett.*, *255*, 133–147, doi:10.1016/j.epsl.2006.12.011.

Karig, D. E., and W. Jensky (1972), The proto-gulf of California, *Earth Planet. Sci. Lett.*, *17*, 169–174, doi:10.1016/0012-821X(72)90272-5.

Kirby, S. H., and A. K. Kronenberg (1987), Rheology of the lithosphere:selected topics, *Rev. Geophys.*, *25*, 1219–1244, doi:10.1029/RG025i006p01219.

Lachenbruch, A. H., and J. H. Sass (1977), Models of an extending lithosphere and heat flow in the Basin and Range Province, in *Cenozoic Tectonics and Regional Geophysics of the Western Cordillera*, edited by R. B. Smith and G. P. Eaton, *Mem. Geol. Soc. Am.*, *152*, 209–250.

Lavier, L. L., and R. Bennett (2006), The tectonics and strength of the San Andreas Fault, *Eos Trans. AGU*, *87*(52), Fall Meeting Suppl., Abstract T43D-1669.

Lavier, L. L., and W. R. Buck (2002), Half graben versus large-offset low-angle normal fault: Importance of keeping cool during normal faulting, *J. Geophys. Res.*, *107*(B6), 2122, doi:10.1029/2001JB000513.

Lavier, L. L., W. R. Buck, and A. N. B. Poliakov (2000), Factors controlling normal fault offset in an ideal brittle layer, *J. Geophys. Res.*, *105*, 23,431–23,442, doi:10.1029/2000JB900108.

Lee, J., M. M. Miller, R. Crippen, B. Hacker, and J. L. Vazquez (1996), Middle Miocene extension in the Gulf Extensional Province, Baja California: Evidence from the southern Sierra Juarez, *Geol. Soc. Am. Bull.*, *108*, 505–525, doi:10.1130/0016-7606(1996)108<0505:MMEITG>2.3.CO;2.

Lizarralde, D., et al. (2007), Variable styles of rifting in the Gulf of California, *Nature*, *448*, 466–469, doi:10.1038/nature06035.

Makris, J. (1978), The crust and upper mantle of the Aegean region from deep seismic soundings, *Tectonophysics*, *46*, 269–284, doi:10.1016/0040-1951(78)90207-X.

McDougall, K. A., R. Z. Poore, and J. C. Matti (1999), Age and paleoenvironment of the Imperial Formation near San Gorgonio Pass, southern California, *J. Foraminiferal Res.*, *29*, 4–29.

McKenzie, D. (1978), Active tectonics of Alpine-Himalayan Belt—Aegean Sea and surrounding regions, *Geophys. J. R. Astron. Soc.*, *55*, 217–254.

Noble, L. F. (1941), Structural features of the Virgin Spring area, Death Valley, California, *Geol. Soc. Am. Bull.*, *52*, 941–1000.

Oskin, M., and J. Stock (2003), Marine incursion synchronous with plate-boundary localization in the Gulf of California, *Geology*, *31*, 23–26, doi:10.1130/0091-7613(2003)031<0023:MISWPB>2.0.CO;2.

Persaud, P., J. M. Stock, M. S. Steckler, A. Martín-Barajas, J. B. Diebold, A. González-Fernández, and G. S. Mountain (2003), Active deformation and shallow structure of the Wagner, Consag, and Delfín basins, northern Gulf of California, Mexico, *J. Geophys. Res.*, *108*(B7), 2355, doi:10.1029/2002JB001937.

Rollet, N., J. Déverchère, M.-O. Beslier, P. Guennoc, J.-P. Réhault, M. Sosson, and C. Truffert (2002), Back arc extension, tectonic inheritance, and volcanism in the Ligurian Sea, western Mediterranean, *Tectonics*, *21*(3), 1015, doi:10.1029/2001TC900027.

Sonder, L. J., and P. C. England (1989), Effects of a temperature-dependent rheology on large-scale continental extension, *J. Geophys. Res.*, *94*, 7603–7619, doi:10.1029/JB094iB06p07603.

Steckler, M. S., and A. B. Watts (1980), The Gulf of Lion: Subsidence of a young continental margin, *Nature*, *287*, 425–429, doi:10.1038/287425a0.

Stock, J. M., and K. V. Hodges (1989), Pre-Pliocene extension around the Gulf of California and the transfer of Baja California to the Pacific Plate, *Tectonics*, *8*, 99–115, doi:10.1029/TC008i001p00099.

Turcotte, D. L., and G. Schubert (2002), *Geodynamics*, 2nd ed., Cambridge Univ. Press, Cambridge, U. K.

Van Andel, T. H. (1964), Recent marine sediments of Gulf of California, in *Marine Geology of the Gulf of California*, edited by T. H. Van Andel and G. G. Shor, *AAPG Mem.*, *3*, 216–301.

Wernicke, B. (1981), Low-angle normal faults in the Basin and Range Province: Nappe tectonics in an extending orogen, *Nature*, *291*, 645–648, doi:10.1038/291645a0.

Willett, S., C. Beaumont, and P. Fullsack (1993), Mechanical model for the tectonics of doubly vergent compressional orogens, *Geology*, *21*, 371–374, doi:10.1130/0091-7613(1993)021<0371:MMFTTO>2.3.CO;2.

R. W. Bialas and W. R. Buck, Lamont-Doherty Earth Observatory, Earth Institute at Columbia University, 305D Oceanography, 61 Route 9W, Palisades, NY 10964, USA. (rbialas@ldeo.columbia.edu)